THE JOURNAL OF IMMUNOLOGY

Epitope Recognition by Diverse Antibodies Suggests Conformational Convergence in an Antibody Response

This information is current as of May 26, 2011

Deepak T. Nair, Kavita Singh, Zaved Siddiqui, Bishnu P. Nayak, Kanury V. S. Rao and Dinakar M. Salunke

J Immunol 2002;168;2371-2382

References This article **cites 45 articles**, 11 of which can be accessed free at:
http://www.jimmunol.org/content/168/5/2371.full.html#ref-list-1

Article cited in:
http://www.jimmunol.org/content/168/5/2371.full.html#related-urls

Subscriptions Information about subscribing to *The Journal of Immunology* is online at
http://www.jimmunol.org/subscriptions

Permissions Submit copyright permission requests at
http://www.aai.org/ji/copyright.html

Email Alerts Receive free email-alerts when new articles cite this article. Sign up at
http://www.jimmunol.org/etoc/subscriptions.shtml/

The Journal of Immunology is published twice each month by
The American Association of Immunologists, Inc.,
9650 Rockville Pike, Bethesda, MD 20814-3994.
Copyright ©2002 by The American Association of Immunologists, Inc. All rights reserved.
Print ISSN: 0022-1767 Online ISSN: 1550-6606.

Downloaded from www.jimmunol.org on May 26, 2011

Epitope Recognition by Diverse Antibodies Suggests Conformational Convergence in an Antibody Response[1]

Deepak T. Nair,* Kavita Singh,* Zaved Siddiqui,† Bishnu P. Nayak,† Kanury V. S. Rao,† and Dinakar M. Salunke[2]*

Crystal structures of distinct mAbs that recognize a common epitope of a peptide Ag have been determined and analyzed in the unbound and bound forms. These Abs display dissimilar binding site structures in the absence of the Ag. The dissimilarity is primarily expressed in the conformations of complementarity-determining region H3, which is responsible for defining the epitope specificity. Interestingly, however, the three Abs exhibit similar complementarity-determining region conformations in the Ag binding site while recognizing the common epitope, indicating that different pathways of binding are used for Ag recognition. The epitope also exhibits conformational similarity when bound to each of these Abs, although the peptide Ag was otherwise flexible. The observed conformational convergence in the epitope and the Ag binding site was facilitated by the plasticity in the nature of interactions. ***The Journal of Immunology,*** **2002, 168: 2371–2382.**

The primary function of the humoral immune response concerns recognition and neutralization of the foreign Ags by Abs. Three-dimensional structures of the mAbs and their complexes with the corresponding Ags of diverse origins have provided critical insights regarding humoral immune recognition (1–3). These studies have contributed immensely toward the understanding of different aspects of an immune response, such as repertoire shift, affinity maturation, idiotype networks, and cross-reactivity (4–8). However, the mechanistic aspects of Ag recognition and neutralization in a polyclonal response would be best studied at the level of an ensemble of Abs recognizing the same Ag.

Complexes of different Abs raised against the same protein Ag, but recognizing independent epitopes, have enabled mapping the antigenic determinants (9–12). Although remarkable structural insights have been gained from all these studies, the correlation of structural information with the mechanistic aspects of a polyclonal Ab response requires further exploration. It has been observed that different extents of conformational changes occur in Abs as well as Ags on binding (1). The role of such changes in defining an immunodominant epitope needs to be further addressed. The immunodominant nature of an epitope manifests itself due to the relatively high immunogenicity of that epitope. Despite the extensive structural work on the Ag-Ab interactions, the structural basis of immunodominance is still a puzzle.

To relate structural, mechanistic, and functional aspects of the humoral immune response, we have used a panel of murine mAbs derived from the secondary response to a peptide Ag, PS1 (HQLD PAFGANSTNPD). All these Abs recognized a common four-residue stretch (DPAF) as an immunodominant epitope. The immune response against this peptide, derived from the large surface Ag of the hepatitis B virus, has been extensively characterized (13). The three mAbs selected for structural studies were derived from the spleen of the highest responder among a group of animals immunized with the peptide PS1CT3, in which CT3 segment of the peptide represents a T cell epitope. The Abs PC283, PC282, and PC287 belong to the isotypes IgG1, IgG3, and IgG1, respectively (14). Furthermore, the differences in the V region sequences, including those of the complementarity-determining regions (CDRs)[3] of both H and L chains of the Abs, are evident (Fig. 1).

The Abs used in this study represent an oligoclonal subset of the polyclonal response mounted against PS1 in an individual animal. The crystallographic analyses of these Abs in their bound and unbound forms should, therefore, provide an insight into the structural features associated with a polyclonal humoral response. Among the three Abs, structure of the complex of PS1 with the Ab PC283 was reported earlier (15). Structure of the bound as well as native forms of the other two Abs, PC282 and PC287, has now been determined. Comparison of the Ag-bound and unbound Ab structures suggests involvement of diverse modes of Ab activation for Ag binding. The ensemble of structures shows that the immune response converges to an equivalent set of CDR conformations recognizing the epitope in a common conformation with uniformly high affinity and specificity. The convergence in conformation of both Ab and Ag observed in this study indicates that the structural repertoire is limited, but effective.

Materials and Methods

Preparation and crystallization of Fab

The IgG was purified by ion exchange chromatography using a salt gradient, followed by cleavage using papain to get Fab (Sigma-Aldrich, St. Louis, MO). Fab molecules were purified from the digestion mixture by ion exchange chromatography using a salt gradient.

All the crystals were obtained in the buffer 50 mM Tris-Cl, pH 7.2, with 0.05% sodium azide. The hanging drop consisted of 5 μl well solution and

*Structural Biology Unit, National Institute of Immunology, and †Immunology Group, International Center of Genetic Engineering and Biotechnology, New Delhi, India

Received for publication September 24, 2001. Accepted for publication January 9, 2002.

The costs of publication of this article were defrayed in part by the payment of page charges. This article must therefore be hereby marked *advertisement* in accordance with 18 U.S.C. Section 1734 solely to indicate this fact.

[1] This work was supported by the funds provided to the National Institute of Immunology by the Department of Biotechnology (government of India). D.T.N. is a recipient of a fellowship from Council for Scientific and Industrial Research (India).

[2] Address correspondence and reprint requests to Dr. Dinakar M. Salunke, Structural Biology Unit, National Institute of Immunology, Aruna Asaf Ali Marg, New Delhi 110067, India. E-mail address: dinakar@nii.res.in

[3] Abbreviations used in this paper: CDR, complementarity-determining region; rmsd, root mean square deviation.

Copyright © 2002 by The American Association of Immunologists

0022-1767/02/$02.00

Downloaded from www.jimmunol.org on May 26, 2011

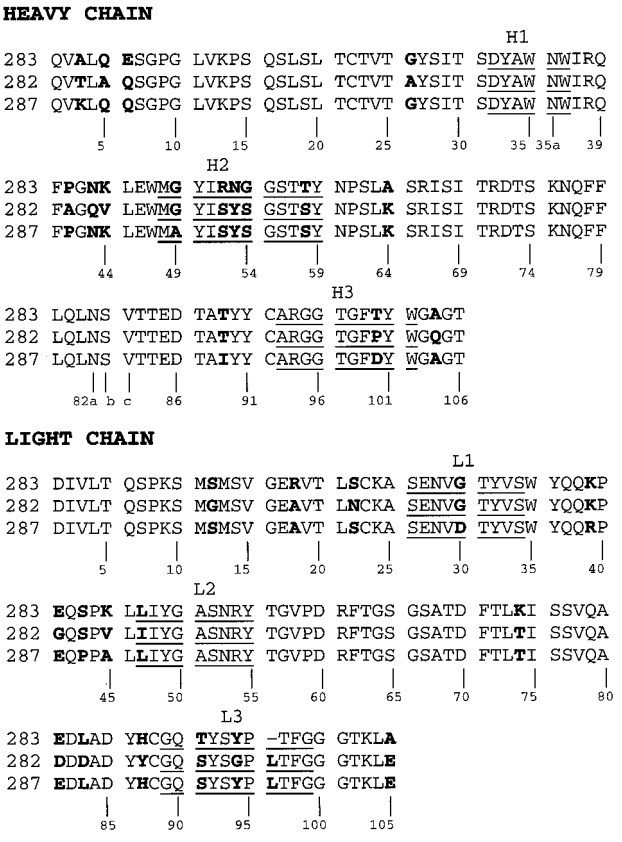

FIGURE 1. Comparison of the V region sequences of the three Abs. The CDRs are labeled and identified by underlining. The differences in the sequence are highlighted in bold. The residue numbering is according to Kabats scheme.

5 μl peptide/Fab (10 mg/ml Fab). For the complexes, peptide:Fab molar ratio of 20:1 was used. Crystals of the PC287 Fab-PS1 and PC282 Fab-PS1 complexes were obtained with a reservoir solution containing 20% PEG3000 and 20% PEG8000, respectively. The crystals of unliganded PC282 and PC287 were grown from a reservoir solution having 10% PEG3000 and 15% PEG8000, respectively. To obtain crystals of PC283 in its native state, crystallization experiments were set up at three different pH values and two different temperatures, using a variety of precipitants, salts, and organic solvents, and using both hanging and sitting drop methods without any success. Microseeding from precipitate and cross seeding also did not lead to crystals.

Data collection

The x-ray intensity data were collected on Image Plate (Marresearch, Hamburg, Germany) installed on a rotating anode x-ray source (RIGAKU) operated at 40 kV and 70 mA (CuKα radiation) with a Ni monochromator. The crystal data and the intensity statistics are shown in Table I. It was inferred from calculations of the Matthews constant (Vm) (16) that there is one molecule in the asymmetric unit for all the crystals. The intensity data were processed using DENZO and merged using SCALEPACK (17).

Structure determination

Molecular replacement was conducted with the PC283 structure as the probe model using AMoRe (18) for both the complexes. The PC282 intensity data gave a good correlation coefficient (C_F = 45.3%), and subsequent refinement was conducted using this model. However, a lower C_F (22.6%) was obtained with PC287-PS1 data. It was envisioned that the relative orientation of the V and H superdomains in the PC287 molecule, defined by its elbow angle, is substantially different from that of the PC283 Fab. Hence, molecular replacement was conducted with a number of different Fab molecules available in the PDB. The model having PDB code 1F58 gave a very good C_F (60%) with the PC287-PS1 intensity data. It was observed, as predicted, that the elbow angle of 1F58 is very different from that of the PC283 Fab. The elbow angle of PC283 was changed to match that of 1F58. Molecular replacement using the modified PC283 Fab structure yielded a C_F of 68%, and, hence, further refinement was conducted using this model.

For the two unliganded datasets, the refined model of each Fab from the complex structures was used to carry out molecular replacement. As expected, a high C_F (~70%) was obtained for both the Abs, and subsequent refinement was conducted using the corresponding models.

Refinement

Further refinement was conducted using CNS (19). Both conventional R_{cryst} and R_{free} (20) values (10% of total reflections) were used to monitor refinement progress. Initially, rigid body refinement was conducted for the

Table I. *Crystal data and refinement statistics*[a]

Property	PC282		PC287	
	Complex	Native	Complex	Native
Space group	$P2_1$	$P2_1$	C2	C2
Cell constants	a = 52.6 Å b = 69.5 Å c = 59.4 Å β = 95.6°	a = 52.6 Å b = 72.9 Å c = 59.6 Å β = 100.5°	a = 73.6 Å b = 71.6 Å c = 87.7 Å β = 98.1°	a = 73.7 Å b = 71.5 Å c = 87.7 Å β = 98.1°
Maximum resolution Å	2.5	1.8	2.5	2.2
Total observations	62432	378203	62464	157194
Unique reflections	14014	36471	13521	14215
R_{merge} (%)	10.2 (47.1)	7.2 (47.1)	10.7 (41.1)	10.0 (51.5)
Completeness (%)	84 (83.2)	91 (83.2)	86 (82.1)	85 (81.8)
Multiplicity	4.5	10.3	4.6	8
Average (I)/(SigI)	4.9 (1.1)	10.5 (3.4)	5.5 (2.1)	6.4 (2.5)
No. of protein atoms	3230	3230	3276	3276
No. of peptide atoms	53	—	68	—
No. of solvent atoms	91	130	158	159
R_{crys} (%)	20.9 (30.9)	20.3 (29.8)	19.7 (37.1)	20 (38.1)
R_{free} (%)	27.7 (32.5)	23.3 (33.4)	27.2 (40.7)	24.9 (40.3)
Refinement range (Å)	50–2.5	50–1.8	50–2.5	50–2.2
rmsd bond lengths (Å)	0.007	0.005	0.007	0.009
rmsd angles (°)	1.529	1.379	1.517	1.593
Ramachandran plot				
Allowed regions (%)	97.4	98.1	96.8	97.6
Generously allowed regions (%)	1.5	1.1	2.4	1.3
Disallowed regions (%)	1.1	0.8	0.8	1.1

[a] The numbers given in parentheses denote the last shell statistics for the corresponding x-ray data or refinement parameter.

Downloaded from www.jimmunol.org on May 26, 2011

whole Fab molecule. On defining V_H, V_L, C_H, and C_L domains as discrete units, the rigid body refinement led to a substantial drop in the R_{cryst} and R_{free}. The model was further refined using positional refinement protocol of CNS. Electron density maps were displayed with the help of program O (21) on O_2 (Silicon Graphics, Mountain View, CA), and the sequence of PC283 was slowly changed to that of the corresponding Abs during iterative refinement. The side chains and backbone conformations of the CDR loops were rebuilt iteratively as the density in these regions improved. Subsequently, clear and empty density could be seen in the Ag-combining site into which the peptide PS1 was gradually built. Initially, the stretch DPAF could be unambiguously fitted into the electron density, and the rest of the peptide could be built subsequently as the refinement progressed. Water molecules were then added using the water__pick program in CNS. The overall quality of the model was checked with PROCHECK (22). For the native structures, a similar refinement protocol was followed. Final refinement statistics for the four structures are given in Table I.

Analysis

The sequence alignment of the V regions of the L and H chains was conducted using CLUSTALW (http://www2.ebi.ac.uk/). The V regions of the three Abs were structurally aligned using the HOMOLOGY module of INSIGHTII (Molecular Simulations, San Diego, CA). The intrapeptide and Ab-peptide contacts were determined using CONTACT program (23). To determine the van der Waals contacts, a cutoff of 4 Å was used. The potential hydrogen bonds listed out by the CONTACT program were confirmed visually in INSIGHTII. The solvent accessible area was calculated using ACCESS__SURF module of MSI software (Molecular Simulations), based on the Lee-Richards algorithm (24), using a probe radius of 1.4 Å. The shape correlation statistic was calculated using program S_c to quantitate complementarity between the DPAF epitope and the three Abs (25). The structures were compared with each other by calculating root mean square deviation (rmsd) in the position of both Cα atoms and all atoms.

Results

Ag structure in different Ab environments

The structure of PS1 bound to PC282 and PC287 were both determined at a resolution of 2.5 Å (Fig. 2). Seven residues from Gln^{2P} to Gly^{8P} and eight residues from His^{1P} to Gly^{8P} could be unambiguously traced into the electron density in the 2Fo-Fc map for the PC282-PS1 and PC287-PS1 complexes, respectively. In both the structures, the conformation of the residues Asp^4-Pro^5-Ala^6-Phe^7 represents a β-turn. The hydrogen bond corresponding to this β-turn is formed between the backbone carbonyl oxygen of Asp^{4P} and backbone nitrogen of Phe^{7P}. This β-turn constitutes the site of primary interactions with the Abs. In the two complexes, the stretch Gln^{2P} to Phe^{7P} is present in the binding site, while the residue Gly^{8P} of the peptide is raised above the Ag-combining site.

The structure of the PC283-PS1 complex in which all the residues of the peptide could be traced into the electron density has already been reported (15). Thus, the stretch QLDPAFG could be unambiguously defined in all the three complexes. To compare the peptide conformations, the PS1 structures were aligned in space by superimposing the V domains of the three Fab molecules. The aligned structures of the common stretch QLDPAFG are shown in Fig. 3*A*. A pairwise comparison of the conformation of the peptide when bound to different Abs was conducted by calculating rmsd values in the position of Cα atoms as well as all atoms. The rmsd values suggest that the side chain and main chain conformation in case of the residues Pro^{5P}, Ala^{6P}, and Phe^{7P} are similar, with all rmsd values being within 0.5 Å. Conformations of the residues Gln^{2P}, Leu^{3P}, Asp^{4P}, and Gly^{8P} are considerably different in case of PS1 bound to PC282 and PC287 compared with the peptide bound to PC283. For Asp^{4P}, the side chain orientation is different in the case of PC283 but similar in the other two complexes. However, the pairwise rmsd values for deviation in the position of Cα atoms of the DPAF stretch are within 0.9 Å. This stretch shows β-turn conformation in all the three complexes (Fig. 3*A*). The presence of a turnlike conformation in peptides bound to Abs has been seen in the structures of a majority of Fab-peptide complexes (1, 15).

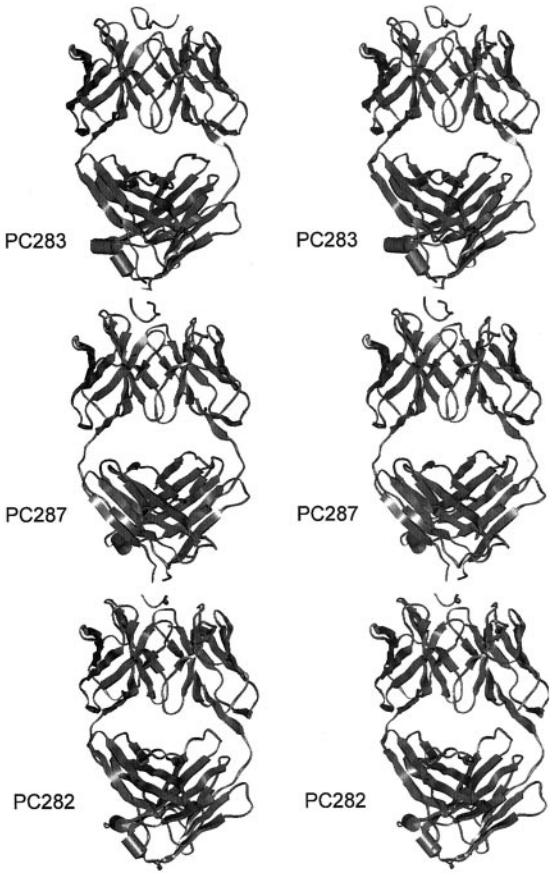

FIGURE 2. Structures of Fab-peptide complexes. Stereoscopic view of the structures of the three Fab-peptide complexes displayed using secondary structure rendering.

Structures of the Abs in the Ag-bound state

The V and C domains are nearly in line with each other in case of PC287, with an elbow angle of 172°. In case of PC283 and PC282, the two superdomains are at an angle with each other, with elbow angles of 147° and 142°, respectively. Thus, the Fab molecules show differences in the relative orientations of the V and C superdomains (Fig. 2). The solvent inaccessible area of the interface between the V_H and V_L domains was measured to be 1594 $Å^2$ in case of PC283, 1488 $Å^2$ in case of PC282, and 1719 $Å^2$ in case of PC287. It has been suggested that the differences in V_H-V_L interface area reflect the differences in the rotational relationships between the two V domains (1, 26). However, the V domain can be superimposed without the need for any transformation on either the V_H or the V_L domain in the three Abs. Thus, the relative orientation of the V_H and V_L domains is the same in the bound forms of all the complexes.

The V domains of the three Abs when structurally aligned according to the strands that compose the β-sheets, as shown in Fig. 3*B*, gave an overall rmsd of 0.5 Å in the position of Cα atoms. A pairwise comparison of the CDR conformations was conducted. The rmsd values in the position of Cα atoms of all the CDRs, except L3, were within 0.5 Å, and hence the variation in their main chain conformation was marginal. Although there are a number of replacement changes in case of CDR L1, H1, and H2, the main chain conformation shows only minor variation. The rmsd values

Downloaded from www.jimmunol.org on May 26, 2011

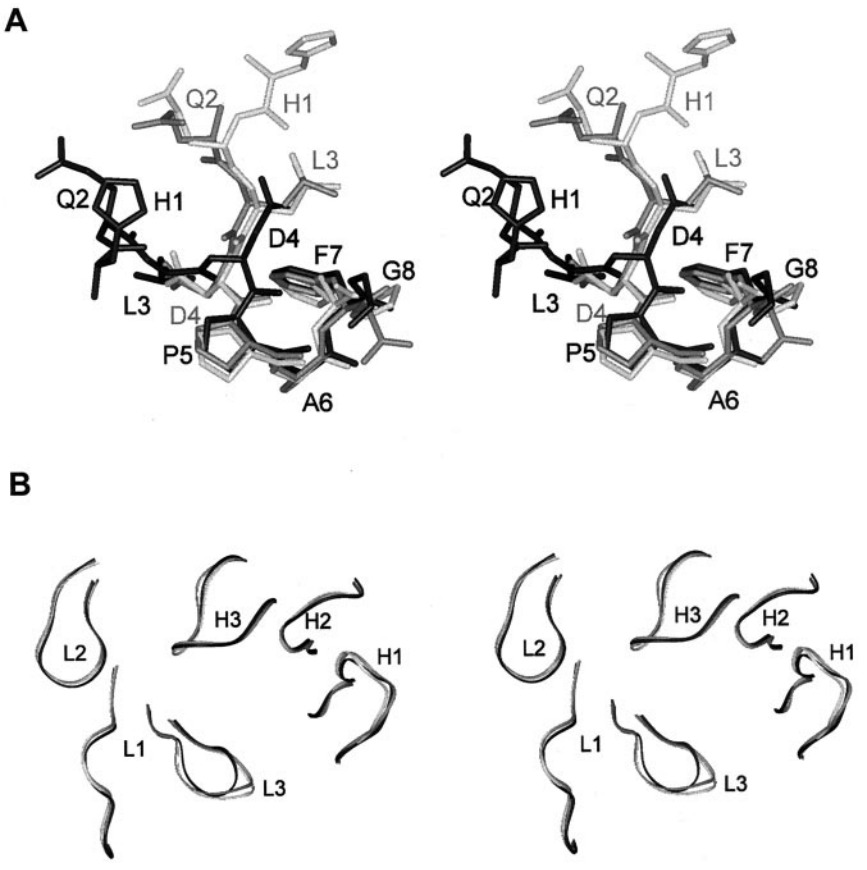

FIGURE 3. The conformational convergence of the epitope and the paratope. *A*, Stereoscopic drawing of the bound conformation for the residues HQLDPAFG of PS1 from the complexes of PS1 with PC283 (black), PC282 (dark gray), and PC287 (light gray). *B*, Stereoscopic drawing of the structural alignment of the CDRs of the three Abs in the bound state, PC283 (black), PC282 (dark gray), and PC287 (light gray).

for Cα atoms of CDR L3 between PC282 and PC283 and between PC287 and PC283 are 2.34 and 2.5 Å, respectively, which are primarily due to an insertion, Leu^{96L}, in CDR L3 in case of PC287 and PC282. The pairwise rmsd values, after exclusion of Leu^{96L} and a residue before and after, were within 0.9 Å, indicating that the major difference in the conformation of CDR L3 is localized near this insertion, with the other residues having similar backbone conformation (Fig. 3*B*).

The V region sequences of the three Abs were compared against the database of mouse V, D, and J germline gene segments using the IgBLAST program (27). For the H chain V gene segment, very high scores were obtained with the genes *VH36–60* and *NC1-A7* in case of all the Abs. For the L chain V gene segment, the genes *19–20* and *19–29* gave high scores with the three Abs. For the H chain J segment, the *JH2* gene, and for the L chain any of the JK genes, except *JK3*, could have been used in each of the three Abs. Among the D segments, *Q52* showed homology with the corresponding region in the H chain of all the Abs. Overall, the CDR sequences of PC282 and PC287 show more similarity to each other than with those of PC283. Although it is possible that the three have originated from independent naive B cells, it is likely that PC283 may have matured from a progenitor distinct from that of the other two Abs.

Ag-Ab interactions

The residues of the three Fab molecules, which show contacts with the peptide residues, are shown in Table II and in Fig. 4. It is obvious from the table that the majority of the interactions in all the three cases are formed by the DPAF stretch of the peptide. The table shows that Leu^{3P} and Asp^{4P} interact with a different set of residues in case of PC287 and PC282 compared with those in case of PC283. The residues of the hypervariable loops that interact with Pro^{5P}, Ala^{6P}, and Phe^{7P} are spatially conserved, and in some cases, are also identical. This is true even for residues of CDR L3, which show a marginally different conformation in the case of PC283 relative to that seen in PC282 and PC287. Furthermore, Table II reveals that the number of contacts formed by the similar Ab residues are slightly different in the three complexes, indicating that there are subtle differences in the conformations of the hypervariable loop and peptide residues.

The hydrogen-bonding interactions between peptide and Ab in case of all the three complexes are shown in Table III. There is a salt bridge formed in case of PC283 between Asp^{4P} side chain and the guanidinium group of Arg^{52H} in the PC283-PS1 complex. In the case of PC282 and PC287, there is a Ser residue at this position in the CDR H2, whose short side chain nullifies any possibility of such an interaction. The side chain of the Asp^{4P} residue forms a hydrogen bond with Ser^{91L}:OH and Gly^{98H}:N in both the cases. The hydrogen bond formed by Ala^{6P}:N with the backbone oxygen atom of the residue present at position L91 is conserved in all three cases. The residue Tyr^{50H} forms hydrogen bonds with different residues of the peptide (Ala^{6P} and Gly^{8P} in the case of PC282 and PC287; Phe^{7P} in the case of PC283) in all three cases.

Water molecules could be placed in the electron density maps of the PC282 and PC287 complexes. In case of PC282-PS1 complex, a water molecule forms hydrogen bonds with Asp^{4P} of peptide and Gly^{50L} of Ab. Even though the residues that are present around this water molecule are the same in both the complexes, the PC287-PS1 complex structure does not show electron density for water at the similar position. The presence of interfacial water molecules at different positions in the same Ab to bind different peptide ligands has been observed earlier

Downloaded from www.jimmunol.org on May 26, 2011

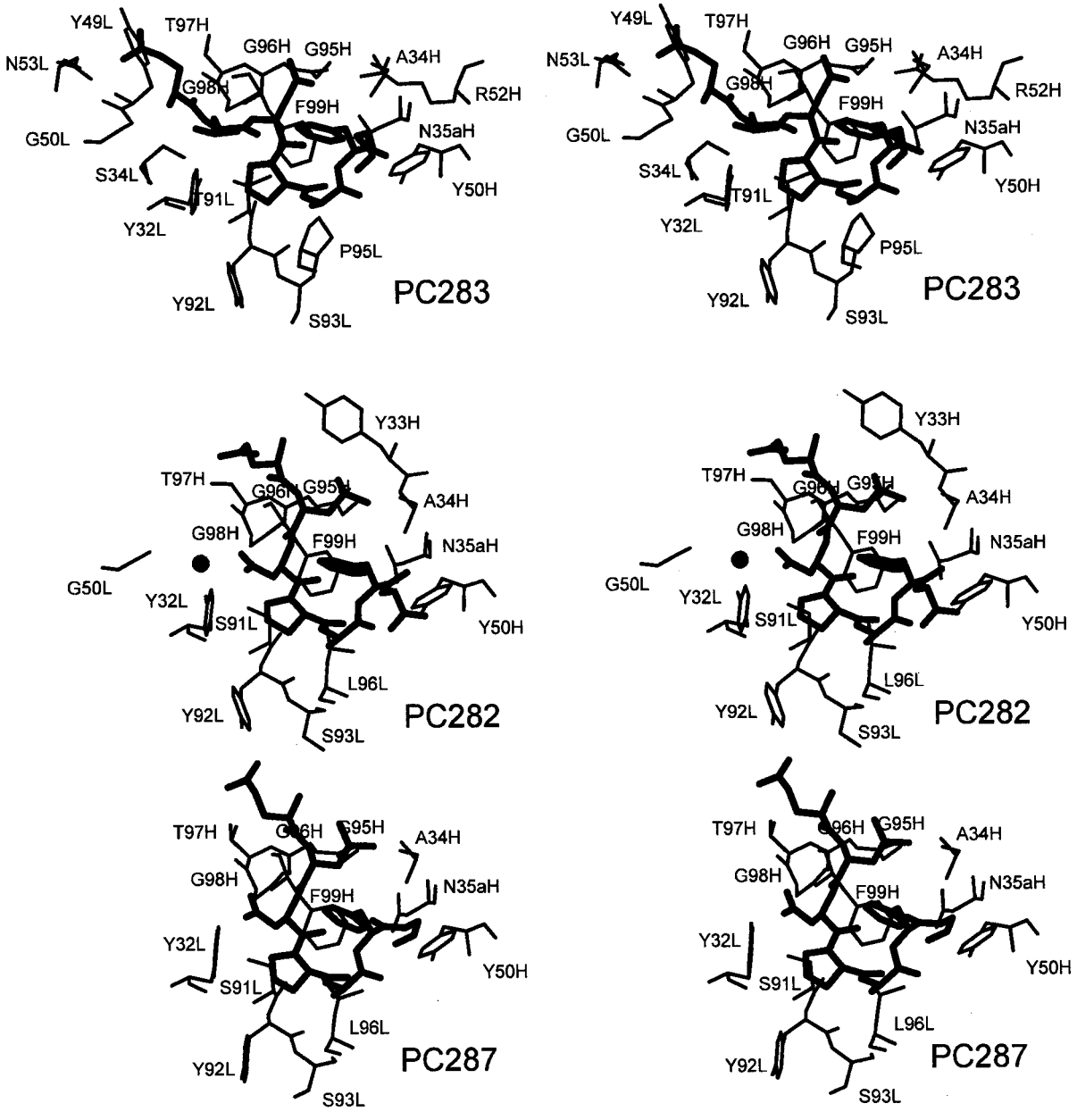

FIGURE 4. Plasticity of the peptide-Ab interactions. Stereoscopic diagram exhibiting interacting residues (within a 4-Å distance) of the three Abs, PC282, PC283, and PC287, shown in thin stick, and the stretch QLDPAFG of PS1 shown in thick stick representation. The bridging water molecule present in case of PC282 is shown as a black circle.

(28). However, in the present case, locally dissimilar interactions, water mediated and otherwise, are used in a similar microenvironment for binding the same ligand in different receptors.

The Ag-combining site (paratope) surfaces are predominantly hydrophobic due to the presence of aromatic amino acids (Fig. 5). This is consistent with the trend that has been observed to date in Ab-Ag complexes (3, 29, 30). In all the three complexes, the epitope is present in a groove in the Ag-combining site, as has been observed for other Ab-peptide complexes (2, 31, 32). The PC283 paratope surface, however, shows a number of features unique from that seen in the other two Abs. The presence of a highly hydrophilic patch (formed by Arg^{52H} with which Asp^{4P} interacts) and a hydrophobic groove (into which Leu^{3P} is inserted) are features unique to PC283 paratope. The features conserved in all the three complexes include the shallow, slightly hydrophobic cavity in which Pro^{5P} is present, the hydrophobic groove in which Ala^{6P} is present, and the hydrophobic cup into which the aryl ring of Phe^{7P} is inserted (Fig. 5). However, it is clear from the figure that the dimensions of the similar topological features in the three complexes do show subtle differences.

The complementarity between the three Abs and the immunodominant epitope DPAF was quantitated by calculating the shape correlation statistics (S_c) (25). The S_c values are calculated to be on a scale of 0 to 1, with the value of 1 indicating maximum complementarity. For the PC283, PC282, and PC287 complexes, the S_c values were 0.76, 0.75, and 0.79, respectively. Hence, the extent of complementarity achieved for the minimal epitope is high and similar in the three Abs.

Downloaded from www.jimmunol.org on May 26, 2011

Table II. *van der Waals contacts between peptide and Ab*[a]

Peptide Residue	PC283 No. of interactions	PC283 Residue	PC282 No. of interactions	PC282 Residue	PC287 No. of interactions	PC287 Residue
His[1P]	8	Y32L (8)		—	4	D32H (4)
Gln[2P]	**12**	**Y49L (4)**		—		
		N53L (2)				
		T97H (6)				
Leu[3P]	**34**	**Y32L (4)**	**6**	**Y33H (2)**	**1**	**G96H (1)**
		Y49L (5)		**G95H (2)**		
		G50L (1)		**G96H (2)**		
		T91L (1)				
		G96H (7)				
		T97H (9)				
		G98H (7)				
Asp[4P]	**3**	**R52H (2)**	**16**	**Y32L (3)**	**19**	**Y32L (8)**
		G96H (1)		**S91L (6)**		**S91L (4)**
				G96H (4)		**G96H (4)**
				T97H (2)		**T97H (3)**
				G98H (1)		
Pro[5P]	**14**	**Y32L (10)**	**7**	**Y32L (4)**	**17**	**Y32L (6)**
		T91L (1)		**S91L (2)**		**S91L (4)**
		Y92L (3)		**Y92L (1)**		**Y92L (7)**
Ala[6P]	**13**	**T91L (3)**	**15**	**S91L (4)**	**12**	**S91L (5)**
		Y92L (3)		**Y92L (5)**		**Y92I (3)**
		S93L (2)		**S93L (2)**		**S93L (1)**
		P95L (1)		**L96L (1)**		**L96L (1)**
		Y50H (4)		**Y50H (3)**		**Y50H (2)**
Phe[7P]	**25**	**T91L (2)**	**21**	**L96L (2)**	**23**	**L96L (3)**
		A34H (4)		**A34H (1)**		**A34H (2)**
		N35aH (1)		**N35aH (2)**		**N35aH (1)**
		Y50H (6)		**Y50H (6)**		**Y50H (3)**
		R52H (1)		**G95H (2)**		**G95H (5)**
		G95H (5)		**G96H (6)**		**G96H (4)**
		G96H (5)		**F99H (2)**		**G98H (1)**
		F99H (1)				**F99H (4)**
Gly[8P]		—	**1[3]**	**Y50H (1)**	**2**	**Y50H (2)**
Ser[11]	17	Y92 (12)				
		S93L (5)				
Thr[12]	21	S93L (8)				
		Y94 (13)				
Asn[13]	18	D1L (7)				
		E27L (2)				
		S93L (6)				
		Y94L (3)				

[a] The interactions shown with the different Abs by the peptide stretch QLDPAFG are highlighted in bold. The total number of interactions formed by each peptide residue is shown in separate columns. The number of interactions shown by each Ab residue is shown in parentheses.

Ab structures in the Ag-free state

The structure of the PC282 Fab molecule in the unliganded native state has been determined at a resolution of 1.8 Å. Cell parameters of the crystals of PC282 in the bound and unbound forms are similar. The elbow angle of the Fab in its native state is 141°, which is two degrees less than that in the bound state. The solvent inaccessible area of the V_H-V_L interface is 1529 Å^2 as compared with 1488 Å^2 in the complex. When the V_H domains in the bound and unbound structures are superimposed, then to overlap the V_L domains a rotational transformation of −4°, 3°, and −3° along *x*-, *y*-, and *z*-axes, respectively, has to be conducted. Thus, there is only a slight rearrangement in the domain organization on Ag binding.

The V domains of the bound and unbound forms were structurally aligned according to the strands that compose the β-sheets, and this alignment is shown in Fig. 6*A*. The rmsd in position of Cα and all atoms of the different CDRs showed that the conformation of L2, H1, and H2 is unchanged on peptide binding. The CDR H3, however, shows a movement of ~4.7 Å. Thus, this CDR undergoes a considerable change in conformation to facilitate peptide binding. The structural alignment of the bound and unbound states of PC282 showed that this CDR moves outward, leading to the formation of the hydrophobic cup in which the aryl ring of Phe[7P] is present. Comparison of the paratope surfaces of the native and bound states shows that there is a significant change on peptide binding, as can also be seen from Fig. 5. The volume of the hydrophobic cup in which Phe[7P] is present is considerably less in the native state. The changes in the CDR H3 conformation constitute a significant rearrangement of the PC282 Ag-combining site on peptide binding. Hence, this binding event can be classified as following the "induced fit" or "handshake" mechanism (33).

The structure of PC287 in the unbound form has been solved to a resolution of 2.2 Å. The unit cell parameters of crystals of the bound and unbound forms are identical. The elbow angle is 172° and does not change on peptide binding. The solvent inaccessible area of the V_H-V_L interface is 1631 Å^2 as compared with 1719 Å^2 in the complex. The alignment of the V domains of PC287 in the bound and unbound structures is shown in Fig. 6*B*. In case of

Downloaded from www.jimmunol.org on May 26, 2011

Table III. *Hydrogen bonding interactions between peptide and Ab*

Peptide Atom	PC283 Atom	PC287 Atom	PC282 Atom
His^{1P}:N	Tyr^{32L}:OH		
Gln^{2P}:NE2	Tyr^{49L}:OH		
Asp^{4P}:N		Gly^{96H}:O	Gly^{96H}:O
Asp^{4P}:OD2	Arg^{52H}:NH2	Gly^{98H}:N	Gly^{98H}:N
		Ser^{91L}:OG	Ser^{91L}:OG
Ala^{6P}:N	Thr^{91L}:O	Ser^{91L}:O	Ser^{91L}:O
Ala^{6P}:O		Tyr^{50H}:OH	Tyr^{50H}:OH
Phe^{7P}:O	Tyr^{50H}:OH		
Gly^{8P}:N		Tyr^{50H}:OH	Tyr^{50H}:OH
Ser^{11P}:OG	Ser^{93L}:OG		
Thr^{12P}:OG1	Tyr^{94L}:OH		

PC287, the rmsd values indicate that the main chain conformations of all the CDRs are the same in both bound and unbound forms, as is evident from Fig. 6*B*. In addition, the values suggest that the side chain conformation of only CDR L3 residues changes significantly on peptide binding. The structural alignment of the bound and unbound states reveals that this is due to the side chain of the residue Tyr^{94L} of CDR L3, which flips outward, away from the Ag-combining site on peptide binding. This residue does not exhibit any interactions with the peptide in the bound state, but its outward flip prevents steric clashes with Ala^{6P} of the peptide. The side chain as well as main chain conformations of the other CDR residues show only minor variations on peptide binding. The paratope surfaces differ significantly between the bound and unbound states primarily due to the conformation of Tyr^{94L}, which is located over the groove in which Ala^{6P} is present in the bound state. The side chain of the Tyr^{94L} also covers the hydrophobic cup in which Phe^{7P} is present to some extent. This hydrophobic cup is also occluded by water molecules present near its rim. The comparison of the bound and native structures suggests that the changes that facilitate ligand binding are the Tyr^{94L} side chain movement and the exclusion of two water molecules. Relative to the substantial rearrangements that are seen in case of PC282, the binding event of PC287 and PS1 follows a lock and key mechanism. It has been proposed earlier that for binding events involving only changes in side chain rotation, the term "mutual fit" is more appropriate (2).

For both PC282 and PC287, the crystal packing in the bound and unbound forms is similar and does not interfere with the conformation of the CDRs in either case. Despite the high sequence identity of CDR H3 between PC282 and PC287 Abs, their behavior on peptide binding is very different. A considerable outward movement of CDR H3 was observed in the former, while the latter showed no conformational change. The analysis of residues involved in stabilizing the paratope structure shows that Pro is present at H100 in case of PC282, while this position is occupied by Asp in PC287. The side chain of Asp^{100H} forms a salt bridge with that of Arg^{94H} and forms hydrogen-bonding interactions with the side chain of Thr^{97H} in both the bound and unbound forms of PC287 (Fig. 7). In case of PC282, however, the Pro residue cannot form such a network of bonds to hold Thr^{97H} in the same position in bound and unbound states. Hence, in the absence of the peptide, the CDR H3 falls toward the center of the groove in the case of PC282. This conformation is stabilized by hydrogen-bonding interactions between backbone carbonyl oxygen of Thr^{97H} and the hydroxyl oxygen of Ser^{91L}. In contrast, in PC287, the network of polar interactions formed between Arg^{94H}, Thr^{97H}, and Asp^{100H} holds the CDR H3 in the same conformation in both absence and presence of peptide.

We were not able to crystallize unliganded PC283 despite multifarious efforts; a large number of conditions and methods have been attempted without any concrete success. It may be noted that

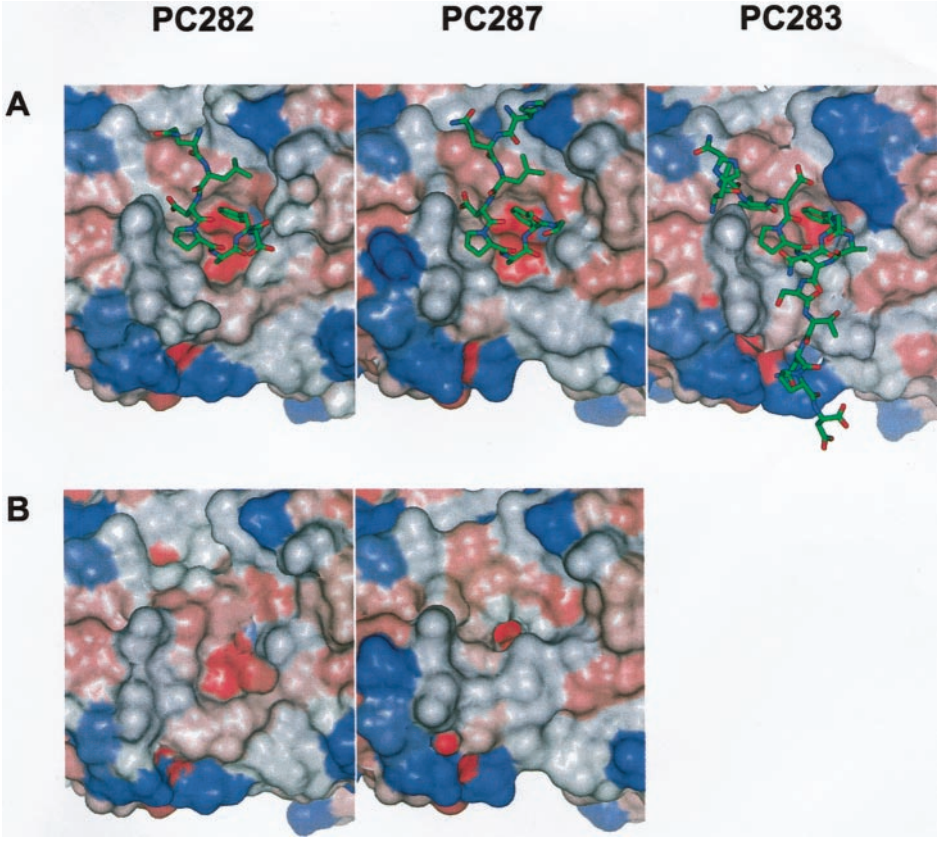

FIGURE 5. Comparison of the surface features of the paratope in bound and unbound forms. The Connolly surface of the Abs decorated with the hydropathy feature with a color spectrum, in which red to blue stands for hydrophobic to charged, respectively, is shown. Peptide is displayed in the stick representation in the bound forms. *A*, PS1 complexed with the Abs. *B*, Native Abs.

Downloaded from www.jimmunol.org on May 26, 2011

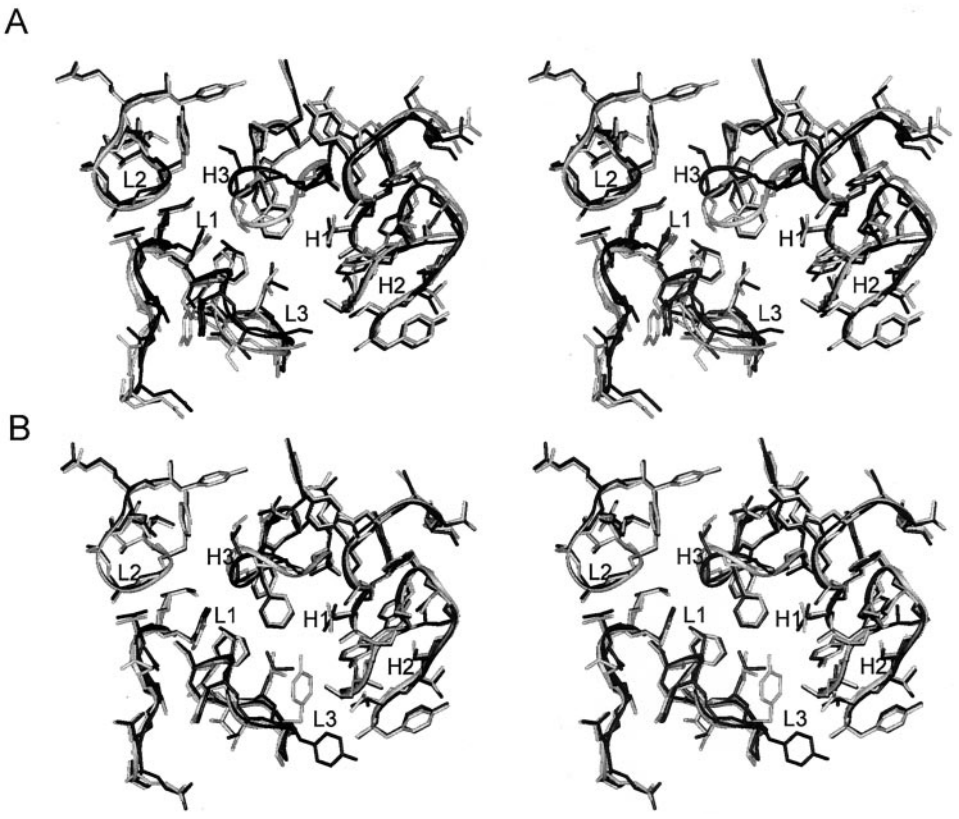

FIGURE 6. Conformational comparison of the Ab paratope in Ag-free and bound forms. Stereoscopic diagram showing superimposition of the CDRs of native (light gray) and complex (black) forms of PC282 (*A*) and PC287 (*B*). The CDR backbone conformations are highlighted by superimposition of the ribbon drawing on the corresponding stick representations.

extensive and unusual interactions between the epitope and paratope were observed in case of PC283-PS1 complex, implying possible role of Ag for stabilizing the paratope structure (15). Therefore, it can be surmised that the Ag-combining site could be flexible in the absence of the Ag in this case. The mechanism of PC283 binding probably involves a disorder-order transition of the CDR loops on ligand binding.

Discussion

Diverse Abs exhibit equivalent topologies while recognizing a common immunodominant peptide epitope in similar conformation

The Fab-peptide crystal structures provide a description of epitope-paratope interactions and conformational features of PS1 when bound to the three independent Abs. In all the complexes, the major energetic contribution to Ab binding of PS1 comes from interactions formed by the four residues DPAF. The murine immune response against PS1 progresses in such a way that, although the primary response is directed against diverse determinants, the Abs in the secondary response are unanimous in their specificity for the stretch DPAF (14). This immunodominant nature of DPAF is in accordance with the observation that the same residues exhibit maximum interactions with the paratope in all the three cases.

For peptide Ags, the inherent flexibility could facilitate adaptability while binding to diverse paratopes from the preimmune repertoire and, thus, be instrumental in eliciting an immune response (34, 35). It was shown that the peptide PS1CT3, against which mAbs were generated, does not have a single definite conformation in aqueous solution, as observed from the proton-decoupled ^{13}C nuclear magnetic resonance and circular dichroism studies (14, 36). PS1 did not indicate propensity for any regular secondary structure, when analyzed experimentally and computationally. Therefore, a priori, it was anticipated that the ability of PS1 to take up a multitude of conformations would be relevant in defining the immunodominant nature of the DPAF epitope. Contrary to this, however, DPAF exists in a similar conformation in all the three complexes.

The DPAF segment adopts a β-turn conformation when bound to any of the three Abs. Diverse peptide epitopes, when bound to corresponding Abs, exist in a variety of different conformations. However, the β-turn conformation is observed statistically more often (1, 15). In the β-turn conformation, all the side chains are directed outward on the same side of the main chain, and the side chains of nonconsecutive amino acids come in close proximity. This enables a large number of side chain interactions with the Ab, ensuring higher specificity. It may, therefore, be inferred that the structural properties that make this particular sequence immunodominant are optimally presented by adopting the β-turn conformation.

Differences exist in the sequences and quaternary arrangements of the superdomains in the three Abs. However, the backbone conformations of the hypervariable loops are remarkably similar in the bound state. In other words, a similar set of CDR conformations is used to stabilize a common conformation of the epitope. It appears that the selection pressures during Ab maturation filter out a common conformational solution to the problem of binding the same epitope. There have been several crystal structures illustrating interactions of Abs with a protein Ag wherein each of the Abs recognizes a different epitope (9). In contrast, the hapten molecules, which are small and rigid, would be expected to bind different Abs in similar orientation exhibiting common interactions. This has indeed been observed in case of two different Abs against a transition state analog hapten derived from the same immune response (37). Unlike proteins and haptens, peptidyl Ags are relatively flexible, and it would have been expected that the polyclonality of the Ab response may actually arise from the conformational polymorphism associated with such linear peptides. Indeed, Churchill et al.

Downloaded from www.jimmunol.org on May 26, 2011

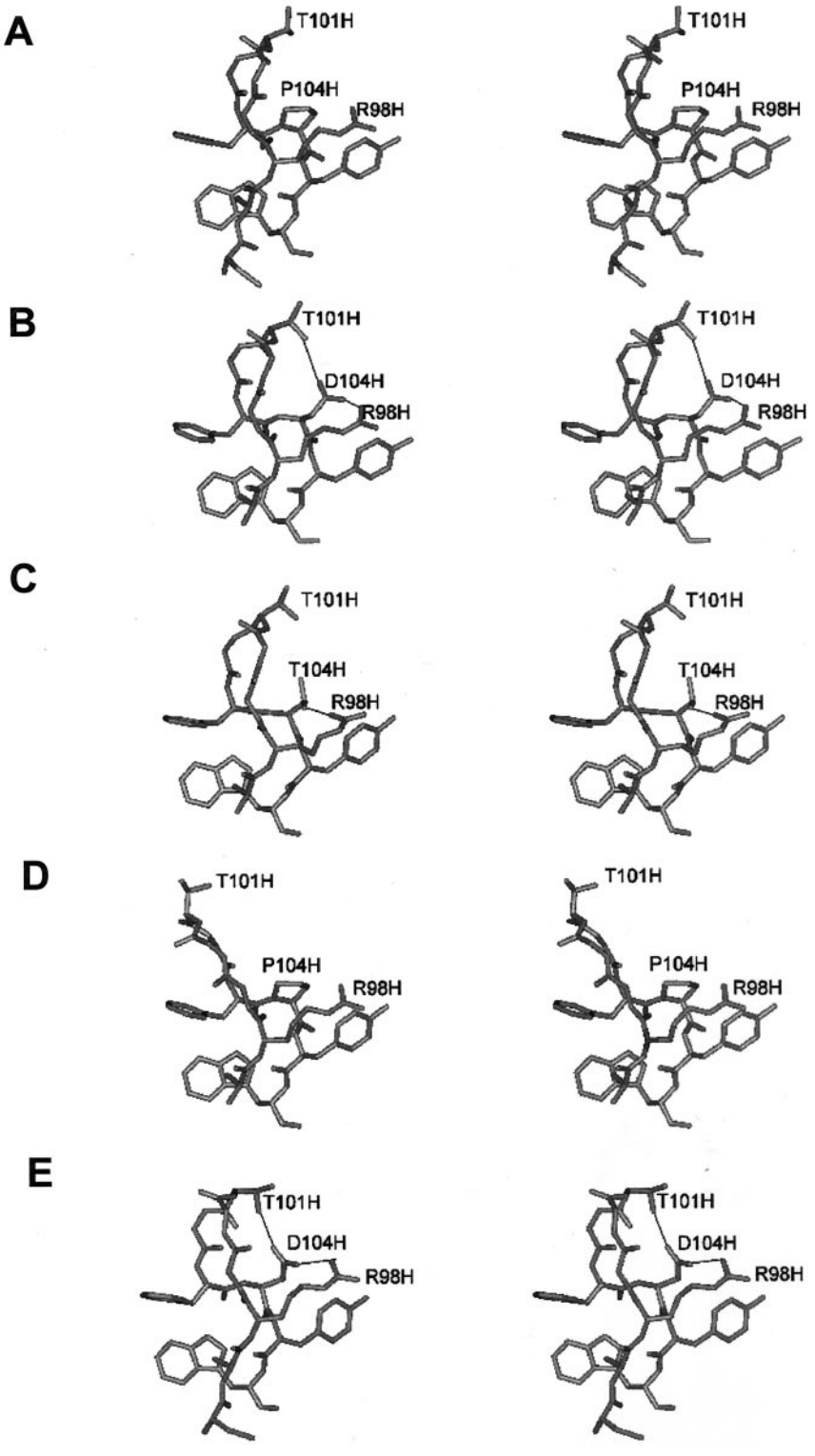

FIGURE 7. Comparison of CDR H3 conformation. Stereoscopic diagrams of the CDR H3 conformation in the three complex structures, PC282 (*A*), PC287 (*B*), and PC283 (*C*), and of the two unliganded structures, PC282 (*D*) and PC287 (*E*). The residues are shown in stick representation, and hydrogen bonds are shown as black lines. The residues critical for structural distinctions are labeled.

(38) have shown that two Abs against a peptide from the hemagglutinin of influenza virus, derived from the same germline progenitor, exhibit similar conformations of the CDRs. In the present study, the three Abs show similar CDR conformations even though they are derived from at least two different germline B cells.

Different pathways of binding are used by diverse Abs for Ag recognition

We have determined the native unliganded structures of two of the three Abs. It is evident that these two Abs show distinct structural

Downloaded from www.jimmunol.org on May 26, 2011

characteristics that are prominently expressed in the CDR H3. It has been established that, among all the CDRs from L as well as H chain, the CDR H3 exhibits maximum sequence and hence conformational variability. Variation in H3 alone is adequate to render protective immunity against diverse pathogens (39). Thus, the structural variations in CDR H3 are essentially designed for defining specificity. It is, therefore, intriguing that such structural variations are observed between PC282 and PC287 in their unliganded form.

Attempts have been made to classify CDR H3 conformations into canonical classes even though this loop adopts a wide range of conformations (40, 41). The part of the loop proximal to the framework region has been referred to as torso, and the tip region has been termed apical. In majority of the cases, presence of an Arg residue at H94 position is a signature for a bulged torso conformation (42, 43). Although the presence of Asp at 100H stabilizes this conformation through a salt bridge with Arg^{94H}, the absence of Asp does not affect this particular conformation of CDR H3. However, from our observations, it appears that presence of Asp at this position in the CDR can influence the apical region conformation. In case of unliganded PC287, the side chain of Asp^{100H} forms a salt bridge with that of Arg^{94H} and shows hydrogen bonding with the side chain of Thr^{97H}. However, because the Asp is replaced by Pro, in case of PC282 this polar interaction is not possible. Accordingly, the CDR H3 falls over the groove in PC282 and is stabilized in an alternate conformation through a hydrogen bond involving backbone carbonyl of Thr^{97H} and the Ser^{91} of CDR L3. In case of PC283, Thr is present at the corresponding position, suggesting a different apical conformation for this loop. Thus, the apical region conformation of CDR H3 would be substantially different in the three Abs, and this can prevent their classification in the same canonical class.

The network of polar interactions formed between Arg^{94H}, Thr^{97H}, and Asp^{100H} holds the CDR H3 in PC287 in the same conformation in both absence and presence of peptide. The absence of such interactions in PC282 leads to a significant difference in the conformation of CDR H3 in the bound and unbound state. Similarly, PC283 also might have a different conformation for this loop in the liganded and unliganded forms. In any case, for PC283, although it could not be crystallized in the Ag-free state, there is indirect evidence to suggest that the paratope in this case may exhibit flexibility. Overall, the sequence differences in the CDR H3 and consequent differences in the polar interactions present in the unbound state lead to different conformations of this CDR in the three Abs. However, on binding the identical epitope DPAF, the conformation of this CDR in the three Abs is similar. There is an explicit shift from different to similar in case of CDR H3 conformation. Hence, when the three Abs are taken together, it is evident that, on epitope stabilization, the CDR H3 converges to a common conformation. In case of the other five CDRs, also it is seen that the rmsd in the position of Cα atoms decreases on peptide binding, albeit to a smaller extent. Thus, the CDRs in the three Abs undergo changes of varying degrees, leading to conformational convergence on Ag binding.

The entire ensemble of structures shows that the core of the peptide-binding groove in the three Abs is highly hydrophobic. In the absence of the Ag, it might, therefore, require shielding from the solvent. Apparently, this is achieved by the movement of CDR H3 over the core of the paratope in case of PC282. Similar conformational change is not possible in case of PC287; this shielding is, therefore, achieved, to an extent, by the flipping of the aromatic ring of Tyr^{94L}. Such a shielding is perfectly achieved on PS1 binding. It can, therefore, be anticipated that the inherent hydrophobic features of the DPAF epitope provide enormous strength in selectivity and may define an additional property relevant for immunodominance in this case.

The three Abs exhibit different levels of structural alterations to ultimately arrive at a similar set of CDR conformations to bind the immunodominant epitope in a common conformation with comparable affinities in the physiological range. They appear to recognize the Ag in three different ways. One involves more of a lock and key mechanism (PC287), the other involves an induced fit mechanism (PC282), and the third probably involves a disorder to order transition (PC283). Even if the two Abs for which we have determined the crystal structure, with bound Ag and without, were to be considered, interesting implications emerge. It is obvious that the paratope is already preorganized for receiving the Ag in one case (PC287), while a significant change in the conformation is necessary in the other (PC282). It is possible that PC282 and PC287 may have matured from the same progenitor. In which case, it is intriguing that they exhibit independent structures in the absence of the Ag and yet converge over to a common structure when bound to the Ag. It has been shown that preorganization of the Ag-combining site can lead to drastic improvement in the affinity during Ab maturation (5). However, in the present case, the affinities exhibited by the two Abs toward the peptide are comparable. The water structure in the vicinity of the paratope is different in the Ag bound and unbound forms of the two Abs. Thus, the reorganization of solvent may have been exploited to compensate for conformational changes to achieve similar binding affinities.

Conformational convergence of Ag-Ab recognition is facilitated by the plasticity of interactions

The complementarity achieved for the minimal epitope is similar in the three Abs. The affinities between the Abs and the epitope, as measured through dissociation constants, have been found to be in the order of 10^{-7} M (44). Thus, the immune system has successfully selected and matured a set of Abs that can bind the DPAF epitope with high specificity and affinity. Structures of the complexes exhibit similar main chain conformation for the epitope as well as the Ab CDRs. There are a number of common interactions in the three complexes. It is seen that the Asp^{4P} residue of the peptide shows a conformational switch to optimally fulfill its potential to form stabilizing interactions. Thus, the flexible nature of the peptide is exploited to compensate for the changes in the paratope to optimize the quality and quantity of Ag-Ab interactions. Also, dissimilar amino acids are present in the three paratopes at equivalent positions interacting with the epitope. A solvent molecule plays a critical role in improving Ag-Ab complementarity in one case, but not in the other two cases. The sequence changes in the paratope may also be compensated, to an extent, through quaternary structural variations in the Ab domains. Thus, there is a degree of plasticity evident in the epitope-paratope association modulated by the nature and conformations of certain side chains and the solvent interactions.

It has been observed earlier that the Ab paratope, especially the germline paratope, does exhibit plasticity (8, 44). The ability of different peptides to bind to the same Ab either by changing structure, or through presence of cementing water molecules, is documented (8, 28). The degree of plasticity seen in the three Fab-peptide complex structures described in this work is qualitatively similar to that observed in other physiological interactions (45, 46). The sequence variations in the CDRs of the three Abs do not lead to significant differences in the main chain conformation due to the observed leeway in interactions. Thus, the conformational convergence of the epitope and the paratopes has direct correlation with the plasticity of Ag-Ab interactions.

Downloaded from www.jimmunol.org on May 26, 2011

Is the structural convergence in epitope-paratope recognition designed for the optimization of immune response?

It is expected that the Ab response in an individual against a flexible epitope would involve a set of genetically heterogeneous Abs, which bind to different parts and conformations of the epitope through diverse CDR conformations and interactions involving different Ab clones. Additionally, it is likely that PC283 could have evolved from a progenitor distinct from that of the other two Abs, and hence two independent naive mature B cells have evolved through somatic mutation into a set of three combining sites. If a flexible peptide binds to separate naive B lymphocytes, one would naturally expect them to lead to independent paratopes. The conformational convergence observed in ours and other related studies gives rise to the hypothesis that the immune system, of an individual mouse, might encourage, against an individual Ag, a single effective binding mode for successful neutralization, resulting in similar conformations of CDRs of different Abs and cognate Ags.

It appears that the immune system evolves high-affinity receptors only to a single conformation of the epitope even though linear peptides adopt multiple conformations in solution. The dominant hydrophobic features in the Ag-binding site may have been responsible for this effect. This could have been achieved by selecting clones with predominantly hydrophobic features and having similar topology to stabilize the common β-turn conformation of the DPAF epitope. Focusing on a single epitope may be an effective and ingenious way of neutralizing the Ag than addressing the conformational repertoire of the Ag in a one-to-one fashion.

The instructional theory regarding Ag-Ab recognition emphasized that the Ab is folded using Ag as a template (47, 48). In the present study, the Abs converge to a common scaffold while binding to a single conformation of the Ag, even though they have different paratope conformations in the unliganded form. This directly relates to the instructional theory and is consistent with the observations made by Wedemayer et al. (5) while comparing the Ag recognition by germline Ab with that by its affinity-matured descendant.

To summarize, in the present study, we examined binding interactions between a conformationally flexible epitope and three distinct Abs. Our finding that there exists conformational convergence of the epitope as well as that of the paratope in all the three cases was particularly surprising. Notably, each of these Abs was found to follow an independent pathway in recognizing the Ag and use a certain level of plasticity to attain the common goal. While the conformational convergence of the epitope could be correlated with its immunodominance, our observation that the Ab also molds itself in accordance with the optimal conformation of the peptide, which is otherwise flexible in solution, describes a unique feature of Ab maturation responses. In addition to this, directed maturation against an energetically favored conformation of an epitope may be an ingenious way of limiting the structural repertoire of the paratope while effectively neutralizing the Ag. It is therefore tempting to suggest that restricted conformational repertoire on Ag binding may be helpful in minimizing the probability of the generation of self-reactive Abs and thus enhancing self/nonself resolution.

References

1. Wilson, I. A., and R. L. Stanfield. 1994. Antibody-antigen interactions: new structures and new conformational changes. *Curr. Opin. Struct. Biol. 4:857.*
2. Webster, D. M., A. H. Henry, and A. R. Rees. 1994. Antibody-antigen interactions. *Curr. Opin. Struct. Biol. 4:123.*
3. Davies, D. R., and G. H. Cohen. 1996. Interactions of protein antigens with antibodies. *Proc. Natl. Acad. Sci. USA 93:7.*
4. Brown, M., M. A. Schumacher, G. D. Wiens, R. G. Brennan, and M. B. Rittenberg. 2000. The structural basis of repertoire shift in an immune response to phosphocholine. *J. Exp. Med. 191:2101.*
5. Wedemayer, G. J., P. A. Patten, L. H. Wang, P. G. Schultz, and R. C. Stevens. 1997. Structural insights into the evolution of an antibody combining site. *Science 276:1665.*
6. Braden, B. C., B. A. Fields, X. Ysern, W. Dall'Acqua, F. A. Goldbaum, R. J. Poljak, and R. A. Mariuzza. 1996. Crystal structure of an Fv-Fv idiotope-anti-idiotope complex at 1.9 Å resolution. *J. Mol. Biol. 264:137.*
7. Bentley, G. A., G. Boulot, M. M. Riottot, and R. J. Poljak. 1990. Three-dimensional structure of an idiotope-anti-idiotope complex. *Nature 348:254.*
8. Keitel, T., A. Kramer, H. Wessner, C. Scholz, J. Schneider-Mergener, and W. Hohne. 1997. Crystallographic analysis of anti-p24 (HIV-1) monoclonal antibody cross-reactivity and polyspecificity. *Cell 91:811.*
9. Bentley, G. A. 1996. The crystal structures of complexes formed between lysozyme and antibody fragments. *EXS 75:301.*
10. Fischmann, T. O., G. A. Bentley, T. N. Bhat, G. Boulot, R. A. Mariuzza, S. E. Phillips, D. Tello, and R. J. Poljak. 1991. Crystallographic refinement of the three-dimensional structure of the FabD1.3-lysozyme complex at 2.5-Å resolution. *J. Biol. Chem. 266:12915.*
11. Padlan, E. A., E. W. Silverton, S. Sheriff, G. H. Cohen, S. J. Smith-Gill, and D. R. Davies. 1989. Structure of an antibody-antigen complex: crystal structure of the HyHEL-10Fab-lysozyme complex. *Proc. Natl. Acad. Sci. USA 86:5938.*
12. Li, Y., H. Li, S. J. Smith-Gill, and R. A. Mariuzza. 2000. Three-dimensional structures of the free and antigen-bound Fab from monoclonal antilysozyme antibody HyHEL-63. *Biochemistry 39:6296.*
13. Rao, K. V. S. 1999. Selection in a T-dependent primary humoral response: new insights from polypeptide models. *APMIS 107:807.*
14. Agarwal, A., S. Sarkar, C. Nazabal, G. Balasundaram, and K. V. S. Rao. 1996. B cell responses to a peptide epitope. I. The cellular basis for restricted recognition. *J. Immunol. 157:2779.*
15. Nair, D. T., K. Singh, N. Sahu, K. V. Rao, and D. M. Salunke. 2000. Crystal structure of an antibody bound to an immunodominant peptide epitope: novel features in peptide-antibody recognition. *J. Immunol. 165:6949.*
16. Matthews, B. W. 1968. Solvent content of protein crystals. *J. Mol. Biol. 33:491.*
17. Otwinowski, Z., and W. Minor. 1997. Processing of X-ray diffraction data collected in oscillation mode. *Methods Enzymol. 276:307.*
18. Navaza, J. 1994. AMoRe: an automated package for molecular replacement. *Acta Crystallogr. A 50:157.*
19. Brünger, A. T., P. D. Adams, G. M. Clore, W. L. DeLano, P. Gros, R. W. Grosse-Kunstleve, J. Jian-Sheng, J. Kuszewski, M. Nilges, N. S. Pannu, et al. 1998. Crystallography and NMR system: a new software suite for macromolecular structure determination. *Acta Crystallogr. D 54:905.*
20. Brunger, A. T. 1993. Assessment of phase accuracy by cross validation: the free R value: methods and applications. *Acta Crystallogr. D 49:24.*
21. Jones, T. A., and M. Kjeldgaard. 1994. *O: The Manual*. Uppsala University, Uppsala.
22. Laskowski, R. A., M. W. MacArthur, D. S. Moss, and J. M. Thornton. 1993. PROCHECK: a program to check the stereochemical quality of protein structures. *J. Appl. Crystallogr. 26:283.*
23. Collaborative Computational Project, Number 4. 1994. The CCP4 suite: programs for protein crystallography. *Acta Crystallogr. D 50:760.*
24. Lee, B., and F. M. Richards. 1971. The interpretation of protein structures: estimation of static accessibility. *J. Mol. Biol. 55:379.*
25. Lawrence, M. C., and P. M. Colman. 1993. Shape complementarity at protein/protein interfaces. *J. Mol. Biol. 234:946.*
26. Stanfield, R. L., M. Takimoto-Kamimura, J. M. Rini, A. T. Profy, and I. A. Wilson. 1993. Major antigen-induced domain rearrangements in an antibody. *Structure 1:83.*
27. Altschul, S. F., T. L. Madden, A. A. Schäffer, J. Zhang, Z. Zhang, W. Miller, and D. J. Lipman. 1997. Gapped BLAST and PSI-BLAST: a new generation of protein database search programs. *Nucleic Acids Res. 25:3389.*
28. Ochoa, W. F., S. G. Kalko, M. G. Mateu, P. Gomes, D. Andreu, E. Domingo, I. Fita, and N. Verdguer. 2000. A multiply substituted G-H loop from foot-and-mouth disease virus in complex with a neutralizing antibody: a role for water molecules. *J. Gen. Virol. 81:1495.*
29. Padlan, E. A. 1990. On the nature of antibody combining sites: unusual features that may confer on these sites an enhanced capacity for binding ligands. *Proteins 7:112.*
30. Stites, W. E. 1997. Protein-protein interactions: interface structure, binding thermodynamics and mutational analysis. *Chem. Rev. 97:1233.*
31. Padlan, E. A. 1996. X-ray crystallography of antibodies. *Adv. Protein Chem. 49:57.*
32. MacCallum, R. M., A. C. R. Martin, and J. M. Thornton. 1996. Antibody-antigen interactions: contact analysis and binding site topography. *J. Mol. Biol. 262:732.*
33. Stanfield, R. L., and I. A. Wilson. 1994. Antigen-induced conformational changes in antibodies: a problem for structural prediction and design. *Trends Biotechnol. 12:275.*
34. Getzoff, E. D., J. A. Tainer, R. A. Lerner, and H. M. Geysen. 1988. The chemistry and mechanism of antibody binding to protein antigens. *Adv. Immunol. 43:1.*
35. Berzofsky, J. A. 1985. Intrinsic and extrinsic factors in protein antigenic structure. *Science 229:932.*
36. Nayak, B. P., R. Tuteja, V. Manivel, R. P. Roy, R. A. Vishwakarma, and K. V. S. Rao. 1998. B cell responses to a peptide epitope. V. Kinetic regulation of repertoire discrimination and antibody optimization for epitope. *J. Immunol. 161:3510.*

Downloaded from www.jimmunol.org on May 26, 2011

37. Buchbinder, J. L., R. C. Stephenson, T. S. Scanlan, and R. J. Fletterick. 1998. A comparison of the crystallographic structures of two catalytic antibodies with esterase activity. *J. Mol. Biol. 282:1033.*
38. Churchill, M. E., E. A. Stura, C. Pinilla, J. R. Appel, R. A. Houghten, D. H. Kono, R. S. Balderas, G. G. Fieser, U. Schulze-Gahmen, and I. A. Wilson. 1994. Crystal structure of a peptide complex of anti-influenza peptide antibody Fab26/9: comparison of two different antibodies bound to the same peptide antigen. *J. Mol. Biol. 241:534.*
39. Xu, J. L., and M. M. Davis. 2000. Diversity in the CDR3 region of V(H) is sufficient for most antibody specificities. *Immunity 13:37.*
40. Oliva, B., P. A. Bates, E. Querol, F. X. Aviles, and M. J. Sternberg. 1998. Automated classification of antibody complementarity determining region 3 of the H chain (H3) loops into canonical forms and its application to protein structure prediction. *J. Mol. Biol. 279:1193.*
41. Morea, V., A. Tramontano, M. Rustici, C. Chothia, and A. M. Lesk. 1998. Conformations of the third hypervariable region in the V_H domain of immunoglobulins. *J. Mol. Biol. 275:269.*
42. Shirai, H., A. Kidera, and H. Nakamura. 1996. Structural classification of CDR-H3 in antibodies. *FEBS Lett. 399:1.*
43. Morea, V., A. Tramontano, M. Rustici, C. Chothia, and A. M. Lesk. 1997. Antibody structure, prediction and redesign. *Biophys. Chem. 68:9.*
44. Manivel, V., N. C. Sahoo, D. M. Salunke, and K. V. S. Rao. 2000. Maturation of an antibody response is governed by modulations in flexibility of the antigen-combining site. *Immunity 13:611.*
45. Chen, L., and P. B. Sigler. 1999. The crystal structure of a GroEL/peptide complex: plasticity as a basis for substrate diversity. *Cell 99:757.*
46. Jain, D., K. J. Kaur, and D. M. Salunke. 2001. Plasticity in protein-peptide recognition: crystal structures of two different peptides bound to concanavalin A. *Biophys. J. 80:2912.*
47. Breinl, F., and F. Haurowitz. 1930. Chemische Untersüchung des Präzipitales aus Hämoglobin und Anti-Hämoglobin-Serum und Bemerkungenüber die Nature der Antikörper. *Z. Phys. Chem. 192:45.*
48. Pauling, L. 1940. A theory of the structure and process of the formation of antibodies. *J. Am. Chem. Soc. 62:2643.*

Downloaded from www.jimmunol.org on May 26, 2011